Properties of $Ni_{38-x}Au_x$-Clusters

Anton Bleckert, Luisa Bleidorn, Jasmin Bunde, Melissa Kirbach, Julia Koch,
Andreas Redondo-Müller, Timo Schulte, Anna Weber and Christina Oligschleger
Department of Applied Science,
Bonn-Rhein-Sieg University of Applied Sciences,
von-Liebig-Str. 20, D-53359 Rheinbach, Germany

December 2023

Abstract

The stability against temperature and the structures of bi-metallic cluster with the composition $Ni_{38-x}Au_x$ and Ni_xAu_{38-x} are investigated using Molecular Dynamics simulations. Structures are heated and equilibrated in stages upto a temperature of 550 K. Properties to account for structures (pair-correlation functions and coordination numbers) and dynamic properties (Lindemann index δ_i) are evualuated.

Molecular Dynamics, metallic Clusters, Nano-Systems

1 Introduction

As metal clusters play a big role in a variety of applications like nucleation and growth of crystals and films, for homogeneous and heterogeneous [1] catalysis [2] or chemistry [3], many different ways of production as well as application dependent certain properties are required. Examples for that are the oxidation reaction of methane or the reduction of CO_2. [4] Recently the synergetic effect of Ni-Au bimetal nanoparticles for the use in hydrogen and arabinose co-production by glucose photoreforming was emphasized. [5] The catalytic activity of metal clusters as well as their physical properties are influenced by the particle size. [1] For some Ni-clusters among others Ni_{38} a magnetic behavior was observed. In large clusters magnetic metals like Ni show in relation to bulk metals lower magnetic moments. Compared to that, large metal clusters out of non-magnetic metals show commonly diamagnetic behavior with much lower moments. [6] As a higher activity, selectivity, stability and resistance to poisoning in heterogeneous catalysis can be reached by using bimetallic instead of single metals this type of cluster gained interest. Rousset et al. studied Au, Ni and AuNi clusters which were produced by laser vaporization of bulk metals and came across with a vanishing of the shift in core level binding energy caused by the size effect (size distribution of pure or alloyed clusters were roughly the same). [7] Further they found out that besides the alloying effect the segregation of gold atoms on the surface causes a shift. As the Au-Ni binary phase diagram shows, no solid solution is present. [7] High resolution electron microscopy and scanning electron microscopy studies on the characterization of bimetallic clusters, among others Au_3Ni and Ni_3Au, also mentioned that Au-Ni systems do not show a solid solution in the bulk phase at ambient temperature. Further it was shown, that the Au-Ni clusters behave like monometallic Au and Ni clusters as the core-level binding energies increase with decreasing coverage or cluster size. The occuring shift in the core-shell levels were seen as the addition of alloying and cluster size effects. [8] The geometric arrangement of the ensemble as well as electronic influences due to the ligands were mentioned as reasons for the

influence of alloying effects on the catalytic properties. [2, 7] The formation of bimetallic clusters (Ni-Au) is independent from the order of deposition. On the surface mainly Au atoms occur as it has a lower surface free energy than Ni and the kinetical limitation of the metal atom mobility through diffusion at room temperature. Is Ni deposited on Au the remaining Ni content on the surface is higher due to a kinetical limited diffusion opportunity within the cluster. [9] As the transformation of the cluster as well as a change in active sides can take place at elevated temperatures it is crucial to investigate the thermal stability of clusters. [4] Schnedlitz et al. investigated the effects of the core location on the strucural stability of Ni-Au core-shell manoparticles and the structural changes choosing higher temperatures. By using MD-simulations they concluded that a decentralized core leads to a promoted diffusion along the intermetallic interface and a quenched intermixing along the radial coordinate. The decentralized Ni core caused an increase of core-shell structure stability. [10] Metal clusters can furthermore be generated in different sizes. Vlachos, Schmidt and Aris investigated small metal clusters with $n = 2-34$ and $n = 55$ at different temperatures with a simulation using the annealing Monte Carlo method. No sharp transition from icosahedral to quasicrystalline could be observed over the (cluster) size as with using the Lennard Jones Potential (sharp transition between $n = 30$ and $n = 31$). This shows that the results can differ depending on the type of body potential that is used while the trend remains the same. With an increase in temperature first restructuring and at higher temperatures isomerization occurs what leads to a change in surface atom coordinates. While Au shows a smooth transition of the coordination number CN with increasing temperature Ni shows a sharp change similar to first order transitions. Using different potentials the abrupt change can occur at larger amounts of atoms. [11] The clusters, which we used in our simulations, are provided by Alvaro Posada-Amarillas (is there a publication, we can refer to?), where different configurations of $Ni_{38-x}Au_x$-clusters are generated and analyzed. From all these configurations we focus on: one $Ni_{37}Au_1$-cluster, two $Ni_{36}Au_2$-clusters, two Ni_2Au_{36}-clusters and three Ni_3Au_{35}-clusters.

2 Methods and Simulations

2.1 Molecular Dynamics

MD simulations represent a valuable link between established theories and experimental observations providing information on a whole raft of equilibrium and dynamic properties of complex systems, including molecular geometries and energies, rates of configurational changes, free energies, *etc* [12]. Therefore, these simulations are also an often preferred choice to evaluate the influence of temperature on the stability of metal clusters, both in terms of structural and dynamical properties [4]. In general, possible applications for MD simulations range from drug discovery to battery development with the latest supercomputers being capable of simulating a million atoms at over $100\,ms$ per day.

To obtain the afore mentioned information and to be able to draw meaningful conclusions from them first the underlying equations of motion have to be solved at every time-step. The solutions to the equations of motion result from a force that in turn is influenced by the parameterization of the underlying force field. For a single atom this context can be expressed as

$$m_i \ddot{r}_i = f_i \qquad\qquad f_i = -\frac{\partial U(R)}{\partial r_i} \tag{1}$$

with mass m_i, acceleration $\ddot{r}_i$, force f_i acting on atom i, and potential energy $U(R)$ [13]. R describes the 3N atomic coordinates with the number of atoms N ($R = (r_1, r_2, ...r_N)$). f_i itself can be calculated by solving the right side of equation 1. For this, a value for $U(R)$ is needed, which in turn is obtained by solving the energy functions implemented within the force field. Commonly used

for atomistic force fields are energy functions for both the bonded interactions

$$\begin{aligned} U(R)_{bonded} = & \frac{1}{2} \sum_{bonds} k_b (b - b_0)^2 \\ & + \frac{1}{2} \sum_{angles} k_\theta (\theta - \theta_0)^2 \\ & + \sum_{dihedrals} k_\phi [1 + \cos(n\phi - \delta)] \end{aligned} \tag{2}$$

and non-bonded interactions

$$U(R)_{non-bonded} = \sum_{LJ} 4\epsilon_{ij} \left[\left(\frac{\sigma_{ij}}{r_{ij}} \right)^{12} - \left(\frac{\sigma_{ij}}{r_{ij}} \right)^{6} \right] + \sum_{Coulomb} \frac{q_i q_j}{r_{ij}} \tag{3}$$

to describe the various interactions between the different atoms [14]. If the equations 2 and 3 are now numerically solved the MD algorithm can then determine the resulting forces acting on each atom and given equation 1 the corresponding change in velocity.

In this work MD simulations were used to study the behavior of 38-atom bimetallic clusters consisting of Au and Ni atoms at different temperatures. Since these are finite systems boundary conditions are not applicable and were thus omitted. The potential used for all the MD simulations was the n-body Gupta potential [15]. For each temperature a total of 250.000 simulation-steps were performed with a time-step of 2 fs.

2.2 Potential

The calculation of potentials is based on the tight-binding second-moment model (TB-SMA), which was defined by Cleri and Rosato [16] to a few free parameters and successfully tested for effectiveness. The tight-binding model is used to calculate ion-ion interactions in solids such as bulks and crystalline structures. Through such a many-body scheme, interfacial effects can be included. While the first moment μ_1 can be assumed to be zero, the binding energy of transition metals can be expressed by $\sqrt{\mu_2}$, which was experimentally proven. The total potential energy E_c consists of two parts, one contribution comes from the

hopping integrals ("overlap" integrals) of d-orbitals in transition metals, these so-called band energy E_B^i of atom i is given by

$$E_B^i = -\left\{ \sum_j \xi_{ab}^2 \exp\left(-2q_{ab}\frac{r_{ij}}{r_0^{ab}} - 1\right)\right\}^{1/2} \tag{4}$$

where i and j are different atoms with a certain distance r. Free parameters of the potential are A, ξ, p, q and r_0. The second contribution results from a short-range interaction between the ions and is necessary for the crystalline stability. The interaction of atom i are described by a Born-Mayer potential:

$$E_R^i = \sum_j A_{ab} \exp\left(-p_{ab}\frac{r_{ij}}{r_0^{ab}} - 1\right) \tag{5}$$

Both contributions are summed up to determine the cohesive energy of the total system:

$$E_C = \sum_i E_B^i + E_R^i \tag{6}$$

In Table 1 we give the element specific parameters for tight binding potentials from the paper of Cleri and Rosato [16].

The simulation is performed under constant pressure (isobar, outer pressure is set to 0 Pa). At the beginning the system is heated from zero to 50 Kelvin. For the heating procedure we scale the velocities of the atoms each time step. Since the simulation takes $500 \cdot 10^{-12}$ seconds (i.e. 250000 time steps) the heating rate results to be 10^{11}K/s. After that, an equilibration at this temperature is performed and the equilibrium simulation also takes 500 ps. The procedure just described, in which the clusters are heated in steps of 50 K and are then equilibrated, is repeated until the clusters are either destroyed or a temperature of 550 K is reached.

2.3 Observables and Properties

The Lindemann index is commonly used to define the melting transition of nanoparticles. [17] Since the focus of the investigations is laid on the structures

of metal clusters and their structural stability we use the Lindemann index as a criterion to account for changes in the vibrational amplitudes of the atoms. This root-mean-square bond fluctuation index is a measure of thermally driven molecular disorder defined by an index of intra-atomic spaces, used to discuss the phase transition temperature indication between solid and liquid state. The Lindemann index δ_i is defined as

$$\delta_i = \frac{1}{N-1} \sum_{i \neq j} \frac{\sqrt{\langle r_{ij}^2 \rangle - \langle r_{ij} \rangle^2}}{\langle r_{ij} \rangle} \tag{7}$$

here, r_{ij} is the distance between atoms i and j, N is the number of atoms in the discussed particle and the brackets represent time averages of the sample's temperature. Therefore, we calculate the Lindemann indices during the equilibrium steps of the simulation runs. In order to observe a change in the atomic dynamics (due to relaxations, diffusions, etc.) over the course of an temperature equilibration period, we divided the entire run into successive time slots, for which we calculate the index δ_i. The total observation period is divided into five sections of equal length and for each section the mean values of distances $\langle r_{ij} \rangle$ and squares $\langle r_{ij}^2 \rangle$ are calculated.

A well-known quantity to gain insight into structural properties either order or disorder of solids and cluster is the pair-distribution function.
We determine the partial pair-correlation functions $g(r)$ a structural property exhibiting the status of matter

$$g(r) = \left\langle \frac{n(r)}{4\pi r^2 \rho \Delta(r)} \right\rangle \tag{8}$$

With $n(r)$ being the number of atoms at a distance in a sphere with thickness $\Delta(r)$. This sphere is located around a central reference atom. The relative density of atoms in the systems is described by ρ, and the brackets $\langle\rangle$ stand for averaging over configurations calculated throughout the simulation runs. Correlations of pairs of atoms were calculated, Ni-Ni, Ni-Au and Au-Au where applicable. Since a variety of isomers exist, the atoms of the clusters differ in

their spatial arrangements or their connections. To gain insight into the detailed structure the calculation the partial pair-correlation functions is important.

Another measure to account for structural changes is the coordination numbers of the atoms. The coordination number CN can be used to distinguish between ordered and disordered structural arrangements. In a typical fcc-crystal the coordination number is 12, whereas glassy/disordered metals possess coordination numbers of upto 14 atoms. [18] All atoms which have distances $r \leq 1.2 \cdot r_0$ are counted as neighbours and thus contribute to CN (r_0 is the nearest-neighbour distance).

3 Results and Discussion

Ni-rich clusters:
As examples of the simulated Ni-rich clusters one example of a $Ni_{37}Au_1$ cluster and two different structures of $Ni_{36}Au_2$ clusters are chosen.

$Ni_{37}Au_1$:
The $Ni_{37}Au_1$ cluster did not fail up to the maximum simulated temperature of 500 K (see Figure 1, resistance up to a maximum tested temperature of 250 K could also be observed for the cluster type $Ni_{34}Au_4$, which is not further deepened). As can be taken from Figure 2 the pair distributions of Au-Ni and Ni-Ni show an approach from a temperature of 350 K and no further overlapping of neighbouring peaks could be noticed. The cluster seems to be stabilized in a narrow range of probability of stay for the atoms so that the cluster held.

$Ni_{36}Au_2$:
The first cluster is heated in stages (as described in the section Methods and Simulations) upto 300 K. As can be seen from Figure 3 the coordination number did only slightly change up to 200 K, while the position of the atoms stayed the same. One can clearly distinguish three atomic shells. The innermost lying atoms ($r < 2.5$ Å) have a coordination number of 12 (i.e. the value corresponds to the one in a fcc-crystal). The atoms in the second shell (2.5 Å$< r < 3.5$ Å)

have a reduced coordination number (CN = 9). This is due to the fact, that these atoms are neighbours to the innermost lying atoms, but the cluster is too small to provide the necessary number of neighbors from the outer shell. The atoms lying in the outermost shell ($r > 3.5$ Å) have the smallest coordination number (CN = 6), since there are too few neighbours. At 200 K first increase in CN took place at distances of round about 3.6 to 4.4 Å. When 250 K was reached a larger increase in this atom position range could be observed, while for the two lower position ranges a slight shift to larger distances and a decrease in CN could be observed. This shows, that the $Ni_{36}Au_2$ cluster remains in an ordered structure up to 200 K and starts changing to a disordered structure at 250 K. In the 300 K equilibrium step failure occurred and the cluster break into a Ni_2Au_2 and a Ni_{34} fragment each.

The second cluster of this composition is heated in stages upto 550 K. In Figure 4 we show the cluster at T = 550 K just before and after the decay. The temperature dependences of the Ni-Ni-, Au-Ni- and Au-Au-pair distribution are depicted in Figure 5. Upto a temperature of 500 K we can see the broadening of the nearest neighbour peaks. With increasing temperature ($T \geq 200$ K) the ordered character of the cluster decreases since the peaks beyond the next neighbours start to overlap. Especially for the Au-Au distances we observe the two Au-atoms are clearly apart at temperatures below 400 K. At this temperature the gold atoms become nearest neighbour and the instability of the complete cluster grows and ends in a decomposition into two fragments. As an indicator of atomic motions we consider the Lindemann index δ_i for each atom of the cluster. The values of δ_i are plotted versus the positions of the atoms. In Figure 6 the results for δ_i vs. r are given for the simulated temperatures. At temperatures below 150 K the values of δ_i are less than 0.04. At temperatures greater than 200 K we observe a clear increase of δ_i which is a strong hints to an increasing mobility of the atoms. Especially atoms lying in the outer layers (positions $r > 3$ Å) undergo a drastic rise of mobility. For temperatures greater than 350 K the values of δ_i are increasing more rapidly. The changes of the atomic mobility has an impact on the coordination numbers CN of the

atoms. In Figure 7 the coordination numbers are plotted versus the position of the atoms. The atoms in the center of the cluster have the largest number of nearest neighbours (CN $>$ 11). With increasing distance from the center the coordination numbers CN decreases and the outermost lying atoms have the least CN (CN $<$ 9).

Au-rich clusters:

In addition to the Ni-rich clusters of the type $Ni_{38-x}Au_x$ also Au-rich clusters of the type Ni_xAu_{38-x} were simulated. Some selected results are presented in the following sections.

Ni_2Au_{36}

The results of two clusters with the composition Ni_2Au_{36} are presented in this section. The first cluster is heated in stages up to 250 K. In Figure 8 we show the cluster at T = 250 K just before and after the decay.

The temperature dependencies of the Ni-Ni-, Au-Ni- and Au-Au-pair distribution are depicted in Figure 9. At a temperature of 50 K the Ni-Ni-pair distribution is slightly larger than 4 Å. With increasing temperature (T $>$ 50 K) the distance r between the Ni atoms decreases until they become direct neighbors. This is possible since more mobility and flexibility become available at higher temperatures. Above 150 K the distance between the Ni atoms slightly increases again and the peak gets broader. Here, the higher temperatures increase the kinetic energy of the atoms to a point where fluctuations in the atom positions and thus changes in inter-atomic distances become more frequent leading to the broader peaks. The Au-Au-pair distribution initially shows multiple distinct peaks. With increasing temperatures these peaks become broader and start to overlap more and more. This indicates a loss of crystalline and ordered features that progresses until the cluster ultimately decays at T = 250 K. As an indicator of atomic motions we consider the Lindemann index δ_i for each atom of the cluster. The values of δ_i are plotted versus the positions of the atoms. In Figure 10 the results for δ_i vs. r are given for the simulated temperatures. At

temperatures greater the 200 K we observe a clear rise of δ_i which is a results of an increased atom mobility. Especially the atoms in outer layers undergo a drastic increase of mobility. The change in the mobility of the atoms also has an impact on the calculated coordination numbers CN for the atoms. In Figure 11 the coordination numbers are plotted versus the atom positions. It becomes apparent that mostly the atoms located in the center of the cluster have the largest number of nearest neighbors (CN $= 8 - 11$). At higher distances from the center (r > 4 Å) CN decreases below seven and the outermost lying atoms have the lowest CN at CN < 6.

A second Ni_2Au_{36} cluster has been simulated with different starting structure. The structure of the Ni_2Au_{36} cluster became disordered during the heating step to 150 K. Also this cluster type showed an elongation/ a distortion in shape which started in the 200 K heating step and a slightly bean-shape including the two Ni atoms in the middle in the 250 K heating step. Furthermore the breaking behavior was similar to that of the Ni_3Au_{35} clusters. Two fragments of $Au_{23}Ni_1$ and $Au_{13}Ni_1$ each were formed, but failure occurred at 250 K equilibrium for the Ni_2Au_{36} cluster.

Ni_3Au_{35}

Three clusters of this composition have been simulated and are heated upto 200 K. Two configurations of Ni_3Au_{35} show similar failure behavior. Both (of them) failed at 200 K (equilibration and heating step respectively) and broke in similar smaller clusters (fragments) which just differ in one Au atom, containing $Au_{13}Ni_1$ and $Au_{22}Ni_2$ or $Au_{12}Ni_1$ and $Au_{23}Ni_2$, resp. In both configurations the three Ni atoms were placed in the middle of the cluster, which elongated, forming a bean-shaped structure when reaching the 100 K equilibration step (exemplary shown in Figure 12). During heating bending movements and vibrations of the cluster endings took place.

As can be seen from the Lindemann indices δ_i (Figure 13 and Figure 14), the atom motion at 100 K was enhanced and the distances r were increased. This

matches with the observation of the expansion and elongation of the cluster at this temperature.
In correlation with the increased motion, the potential energy at 100 K changed too over the simulation time (Figure 15). Noticeable are sharp peaks. Depending on the position of the atoms in the arrangement and the bending movement of the bean-shaped cluster the potential energy either increased or decreased until the arrangement seems to stabilize after approximately 150000 MDS and 125000 MDS each.

The third cluster $Ni_3Au_{35} - 130$ breaks into two fragments at 150 K. Using the graphic viewer VMD [19] we visualize the structure. Figure 16 (left) shows the cluster at 150 K equilibration. The simulated structure is deformed like a banana or a bean just before it decays. Similar to the other clusters, the three nickel atoms here continue to hang together despite the high atomic motions within the structure. The decay of the structure can be seen in Figure 16 (right). Here, two fragments once with two nickel atoms and with one nickel atom are formed. The nickel atoms have therefore not remained completely together but have distributed over the two parts.

For this cluster the Lindemann index δ_i vs r is shown in Figure 17. At the lowest temperature 50 K, the points are almost all on one line, the further the temperature rises, the more scattered the points are in the diagram. This is an indication that the atoms move more and change their positions due to the temperature increase.
The influence of the increasing temperatures on the coordination numbers can be seen in Figure 18, the coordination number is plotted against the position of the atoms in the cluster for each simulated temperature, resp. As can be seen in other cluster examples, the atoms in the center of the cluster have the largest coordination number (CN ≈ 11). The further away the atoms are from the cluster center, the smaller the coordination numbers become.
In Figure 19 the temperature-dependent pair distributions of Ni-Ni, Ni-Au and

Au-Au atoms are shown. In all three diagrams, the orange curve at 200 K is the most striking. However, the high peaks of these curves only indicate that the cluster has already decayed at this temperature.

4 Summary and Conclusion

We use Molecular Dynamics simulations to investigate the stability of Ni-Au clusters with a total number of 38 atoms. The Ni-rich clusters provide a good stability with temperature. The most temperature resistant clusters have the composition $Ni_{37}Au_1$, clusters of that type did not break apart at the highest applied temperature of 550 K. Clusters with a molecular formula $Ni_{36}Au_2$ possess a reduced temperature resistance and break apart at temperatures between 300 K and 550 K. Results for the type $Ni_{34}Au_4$ are not shown, however we would like to mention, that the increased number of gold atoms causes a further stability decrease against temperature. The $Ni_{34}Au_4$-clusters decay in two parts in a temperature range from 250 K to 500 K. The Au-rich clusters show a much less temperature resistance. The typical temperature for a fragmentation of Ni_2Au_{36} clusters range from 250 K to 300 K whereas clusters of the composition Ni_3Au_{35} decay at temperatures from 150 K to 250 K.

As temperatures rise, the movements of atoms within the clusters increase This can also been observed from Lindemann index δ_i, which has values below 0.05 for the lowest temperatures and has values upto 0.4 in case the clusters break into fragments.

Temperature increase and fragmentation of the cluster are accompanied with disorder of the structural arrangement. The occurrence of disorder can also be seen in the coordination numbers CN and the various partial pair distributions. The coordination numbers CN for the ordered starting configurations show a clear shell structures with well defined number of neighbouring atoms. As structural disorder increases, the shell structure is dissolved. The same applies to the partial pair distribution functions, in which the peaks that are clearly visible at low temperatures overlap with increasing temperatures.

The observation of the potential energy during equilibration reveals the appearance of structures that can be assigned to different minima of the potential energy surface.

References

[1] Jean Bourdon. *Growth and Properties of Metal Clusters: Applications to Catalysis and the Photographic Process - International Conference Proceedings*. Elsevier Science & Technology, San Diego, 2000.

[2] B.C. Gates, L. Guczi, und H. Knözinger. *Metal Clusters in Catalysis*. 29. Elsevier, 1986.

[3] P. Braunstein, L.A. Oro, und P.R. Raithby. *Metal Clusters in Chemistry*. John Wiley & Sons, Inc, 1 edition, 2008.

[4] Oscar Alan Sanders-Gutierrez, Analila Luna-Valenzuela, Alvaro Posada-Borbón, J. Christian Schön, und Alvaro Posada-Amarillas. Molecular dynamics and DFT study of 38-atom coinage metal clusters. *Computational Materials Science*, 201:110908, 2022.

[5] Malin Eqi, Cai Shi, Jiajing Xie, Fuyan Kang, Houjuan Qi, Xushen Tan, Zhanhua Huang, Junli Liu, und Jiang Guo. Synergetic effect of Ni-Au bimetal nanoparticles on urchin-like TiO_2 for hydrogen and arabinose coproduction by glucose photoreforming. *Advanced composites and hybrid materials*, 6(1), 2023.

[6] Günter Schmid. Metallcluster. Studienobjekte der Metallbildung. *Chemie in unserer Zeit*, 22(3):85–92, 1988.

[7] J. L. Rousset, F. J. Cadete Santos Aires, B. R. Sekhar, P. Mélinon, B. Prevel, und M. Pellarin. Comparative X-ray Photoemission Spectroscopy Study of Au, Ni, and AuNi clusters produced by Laser Vaporization of Bulk Metals. *The Journal of Physical Chemistry. B*, 104(23):5430–5435, 2000.

[8] A.K. Santra, G.N. Subbanna, und C.N.R. Rao. An investigation of bimetallic clusters by a combined use of electron microscopy and photoelectron spectroscopy: additive effects of alloying and cluster size on core-level binding energies. *Surface science*, 317(1):259–268, 1994.

[9] Samuel A. Tenney, Wei He, Jay S. Ratliff, David R. Mullins, und Donna A. Chen. Characterization of Pt–Au and Ni–Au clusters on TiO_2(110). *Topics in catalysis*, 54(1-4):42–55, 2011.

[10] Martin Schnedlitz, Ricardo Fernandez-Perea, Daniel Knez, Maximilian Lasserus, Alexander Schiffmann, Ferdinand Hofer, Andreas W. Hauser, Maria Pilar de Lara-Castells, und Wolfgang E. Ernst. Effects of the core location on the structural stability of Ni–Au core–shell nanoparticles. *Journal of Physical Chemistry. C*, 123(32):20037–20043, 2019.

[11] D. G. Vlachos, L. D. Schmidt, und R. Aris. Comparison of small metal clusters: Ni, Pd, Pt, Cu, Ag, Au. *Zeitschrift für Physik D Atoms, Molecules and Clusters*, 26(S1):S156–S158, 1993.

[12] Tamar Schlick. *Molecular modeling and simulation: an interdisciplinary guide*, Band 2. Springer, 2010.

[13] Michael P. et al. Allen. Introduction to molecular dynamics simulation. *Computational soft matter: from synthetic polymers to proteins*, 23(1):1–28, 2004.

[14] Erik R. Lindahl. Molecular dynamics simulations. *Molecular modeling of proteins*, pages 3–23, 2008.

[15] Raju P. Gupta. Lattice relaxation at a metal surface. *Physical Review B*, 23(12):6265, 1981.

[16] Fabrizio Cleri und Vittorio Rosato. Tight-binding potentials for transition metals and alloys. *Physical Review B*, 48:22–33, Jul 1993.

[17] Yikun Peng, Zean Tian, Lulu Liu, und Quan Zheng. Autonomous identification of lindemann atoms based on deep learning. *Materials Today Communications*, 35:106053, 2023.

[18] Dmitri V. Louzguine-Luzgin. Structural Changes in Metallic Glass-Forming Liquids on Cooling and Subsequent Vitrification in Relationship with Their Properties. *Materials*, 15(20):7285, 2022.

[19] William Humphrey, Andrew Dalke, und Klaus Schulten. VMD – Visual Molecular Dynamics. *Journal of Molecular Graphics*, 14:33–38, 1996.

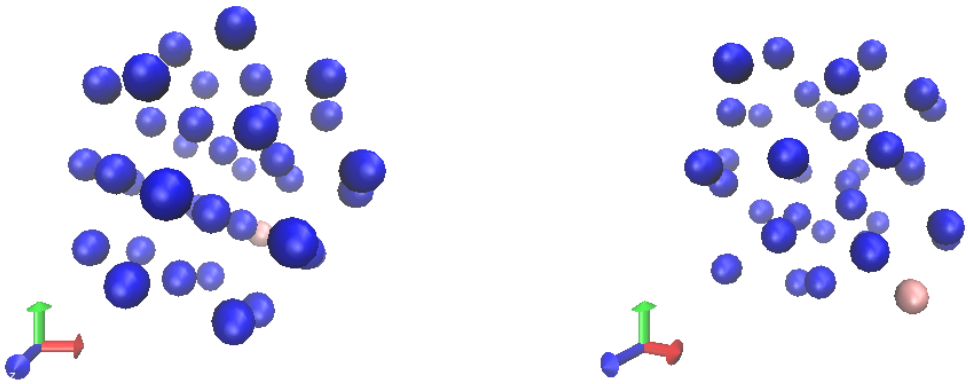

Figure 1: Structures of $Ni_{37}Au_1$ at $T = 50$ K (left) and at $T = 500$ K (right), the atomic coordinations are plotted using the molecular graphics viewer VMD [19].

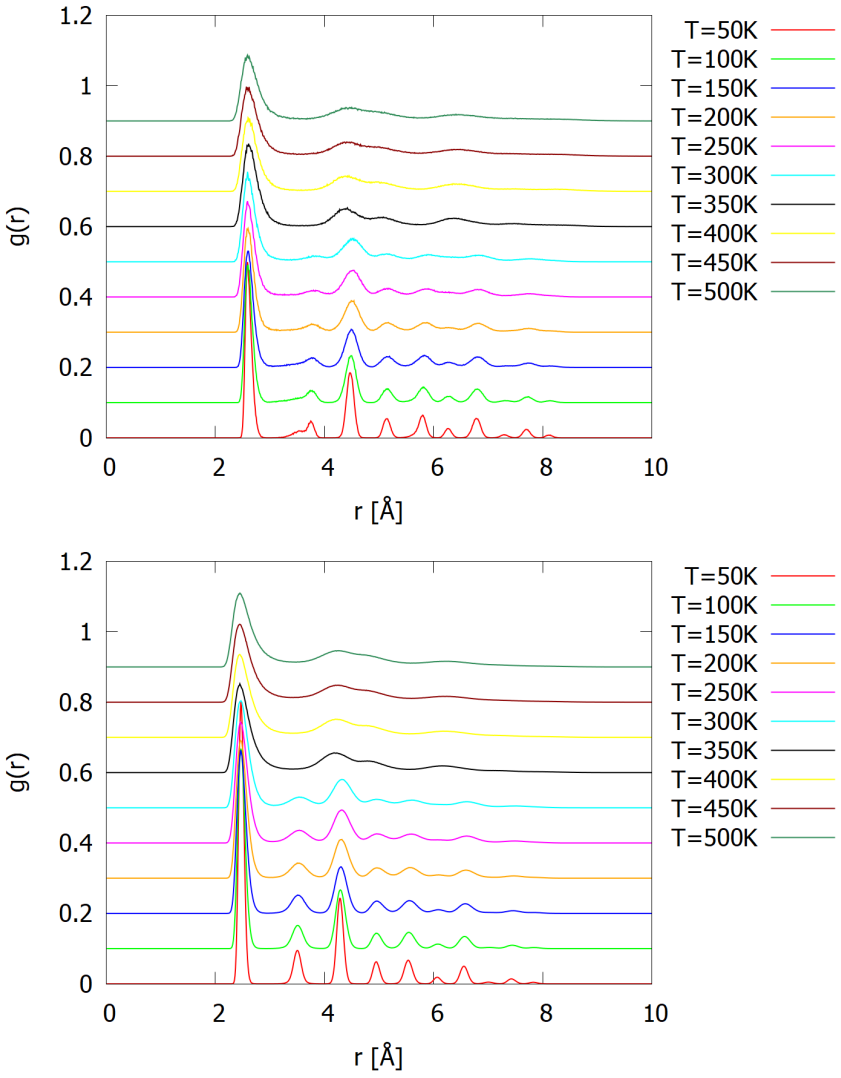

Figure 2: Temperature dependence of the pair distributions of Au-Ni (top) and Ni-Ni (bottom) in the $Ni_{37}Au_1$-cluster, up to the maximum simulated temperature of 500 K.

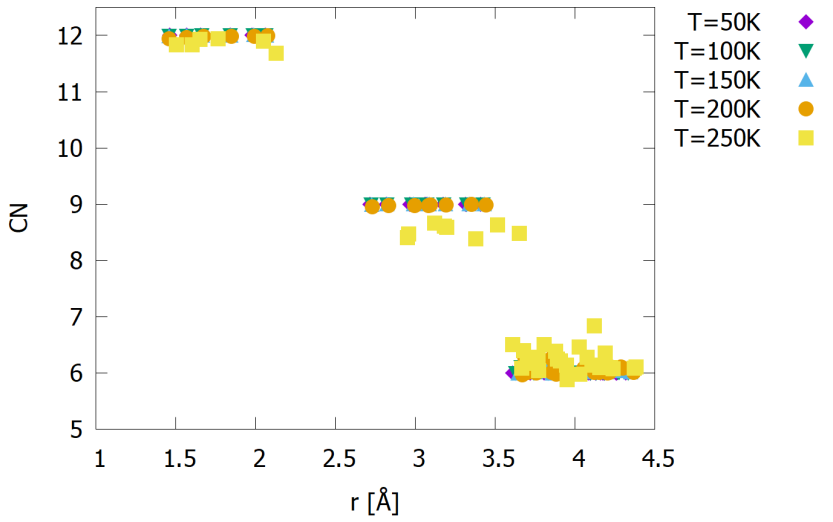

Figure 3: Coordination number CN plotted versus the positions of the atoms at different temperatures.

Figure 4: Structures of $Ni_{36}Au_2$ at $T = 550$ K just before (left) and after (right) the decay.

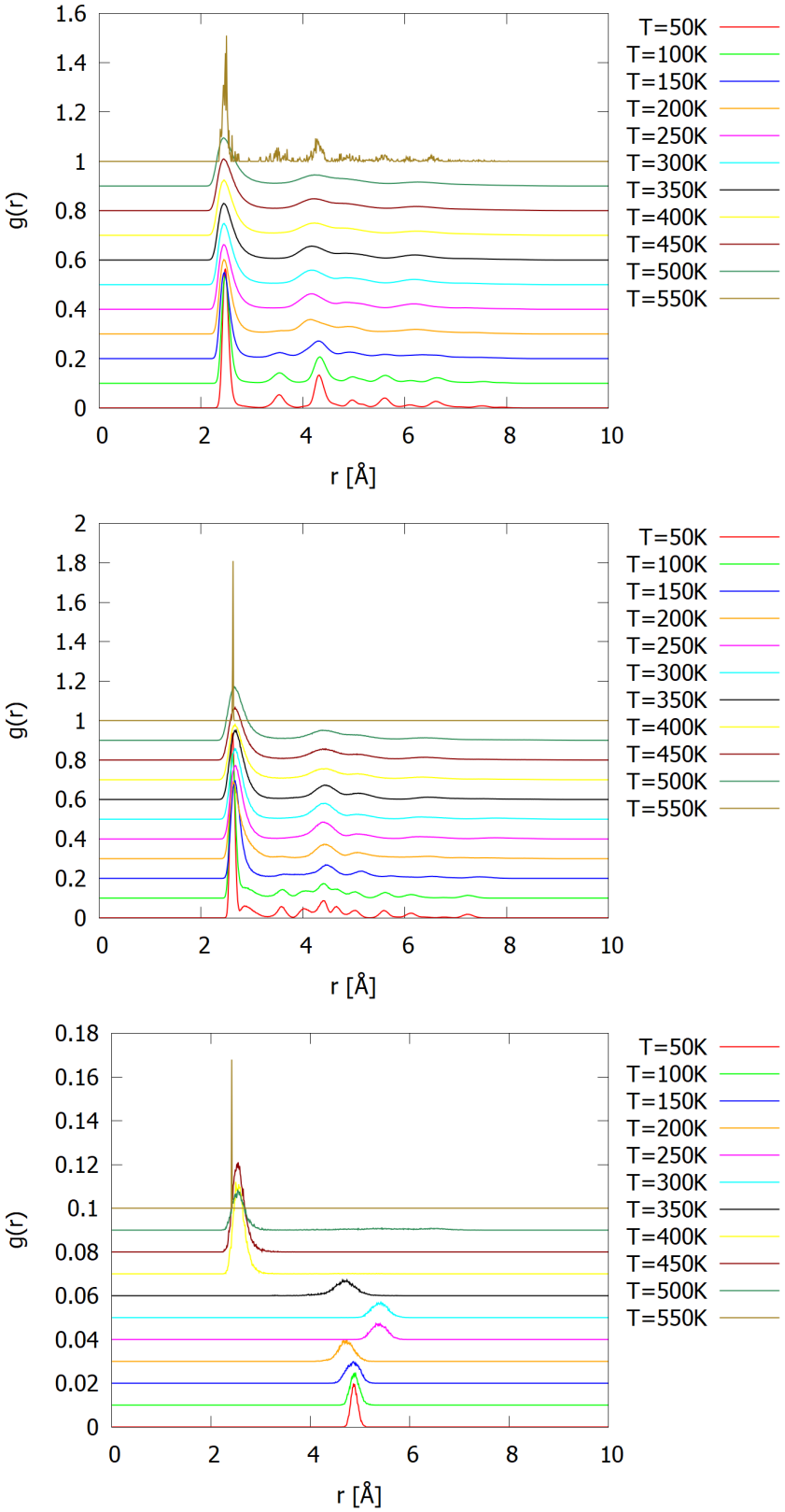

Figure 5: Temperature dependence of the pair distributions of Ni-Ni (top), the Au-Ni (middle) and Au-Au (bottom) of the $Ni_{36}Au_2$-cluster, resp. The heights of the peaks at T=550 K are reduced for clarity, i.e. they are scaled with factors 0.5, 0.5 and 0.05, resp.

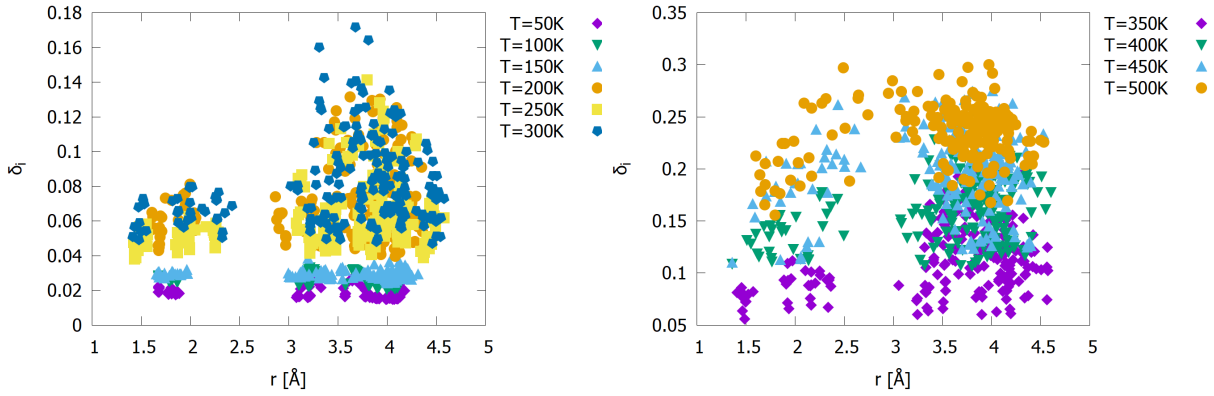

Figure 6: Lindemann index δ_i plotted versus the positions of the atoms at different temperatures, δ_i for T $\leq$ 300 K (left), δ_i for 350 K $\leq$ T $\leq$ 500 K (right).

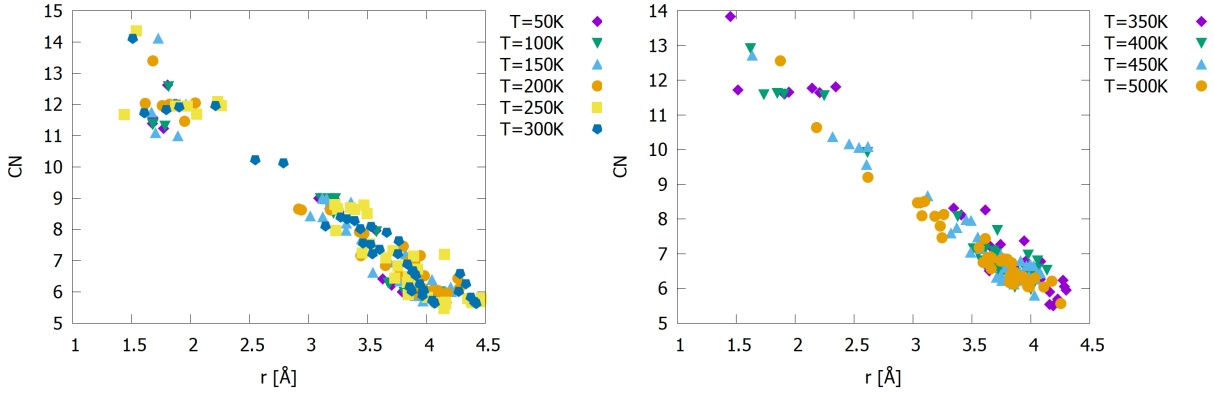

Figure 7: Coordination number CN plotted versus the positions of the atoms at different temperatures, CN for T $\leq$ 300 K (left), CN for 350 K $\leq$ T $\leq$ 500 K (right).

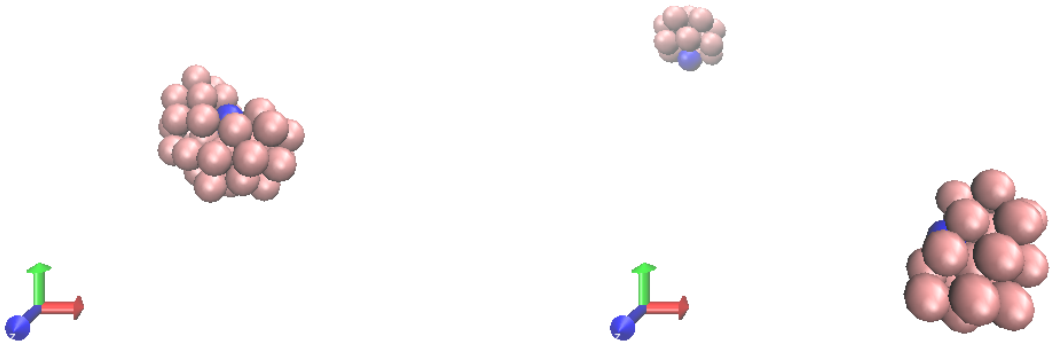

Figure 8: Structures of Ni_2Au_{36} at T=250 K just before (left) and after (right) the decay.

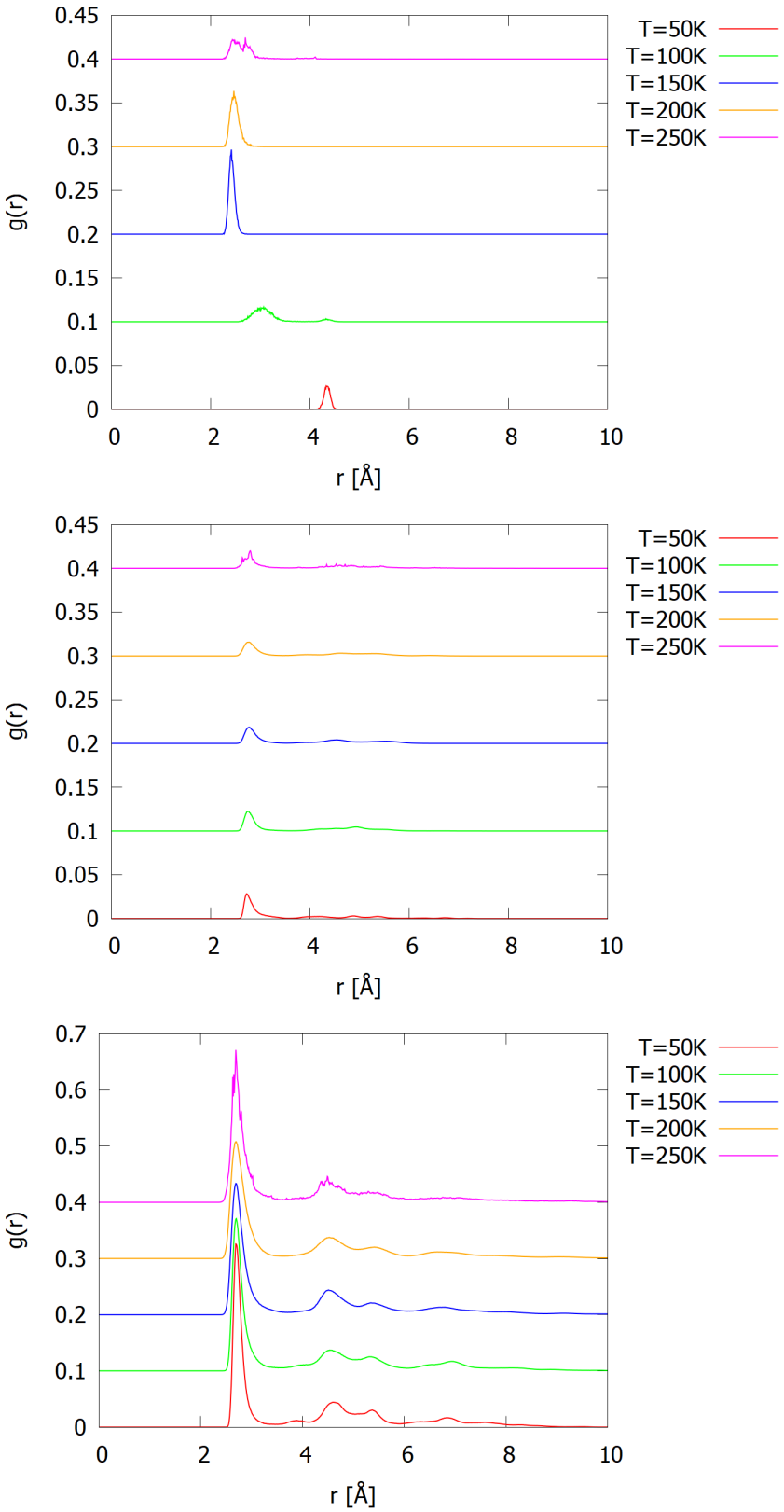

Figure 9: Temperature dependence of the pair distributions of Ni-Ni (top), the Au-Ni (middle) and Au-Au (bottom) for the Ni_2Au_{36}-cluster.

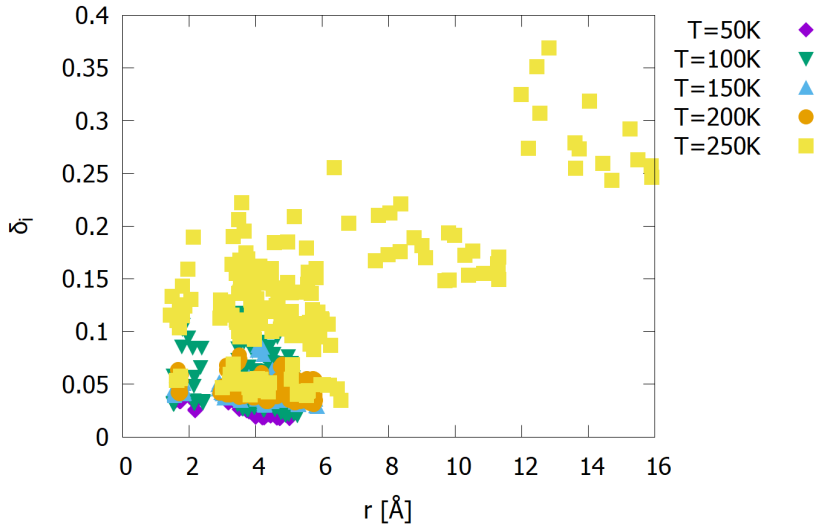

Figure 10: Lindemann index δ_i plotted versus the positions of the atoms at different temperatures.

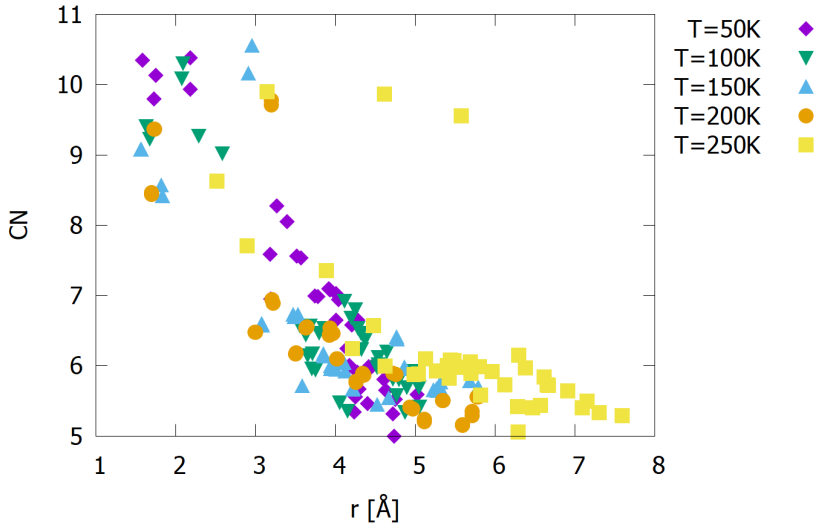

Figure 11: Coordination number CN plotted versus the positions of the atoms at different temperatures.

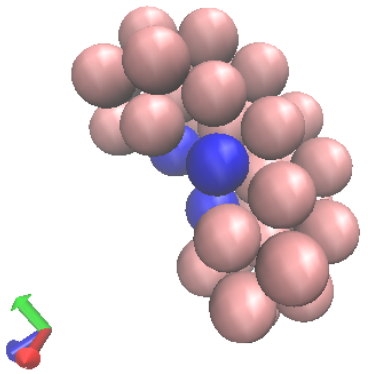

Figure 12: Bean shaped Ni_3Au_{35} cluster at T=150 K equilibrium step

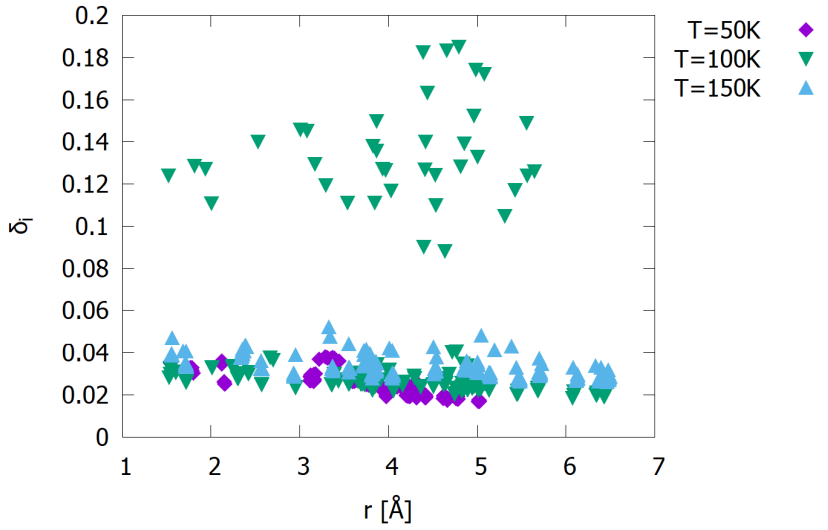

Figure 13: Lindemann index of the Ni_3Au_{35} (111) cluster in a temperature range of 50 K, 100 K and 150 K.

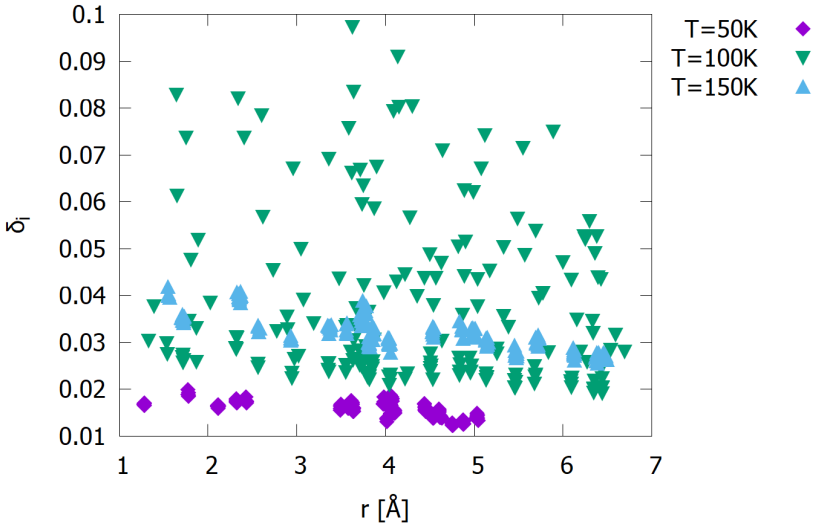

Figure 14: Lindemann index of the Ni_3Au_{35} (105) cluster in a temperature range of 50 K, 100 K and 150 K.

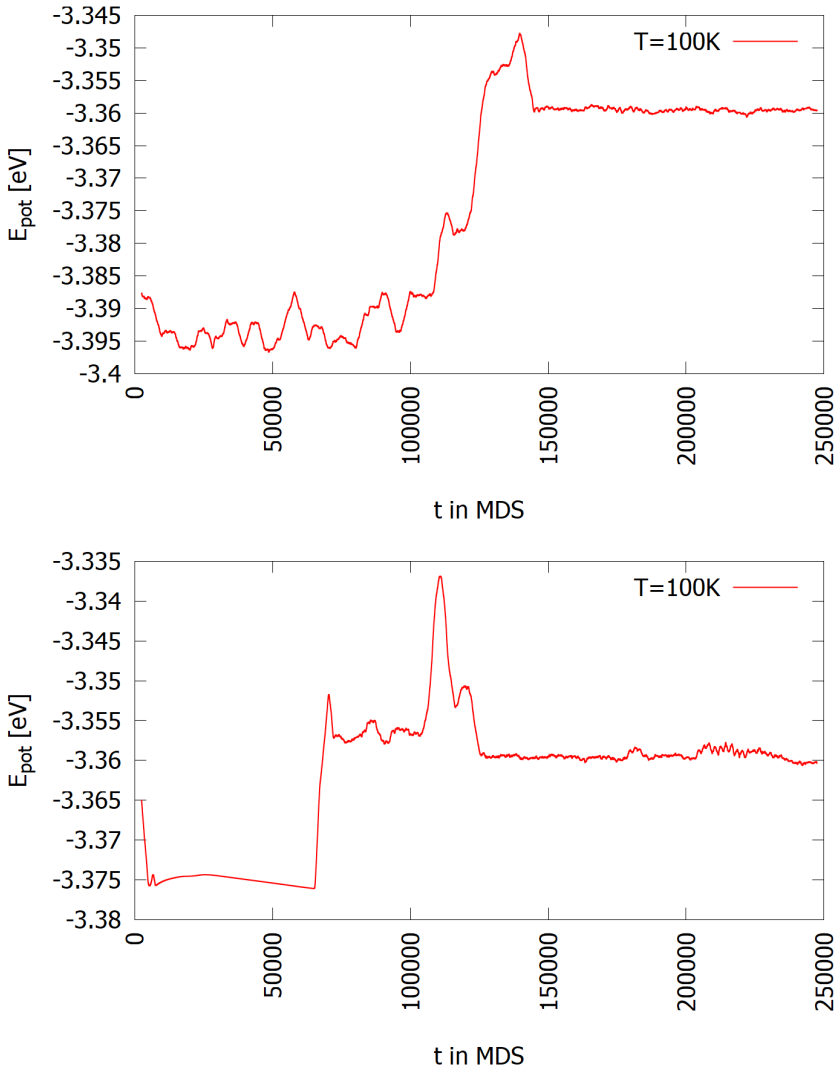

Figure 15: Changes in potential energy over time at 100 K equilibrium for Ni_3Au_{35} (upper diagram (111), lower diagram (105)).

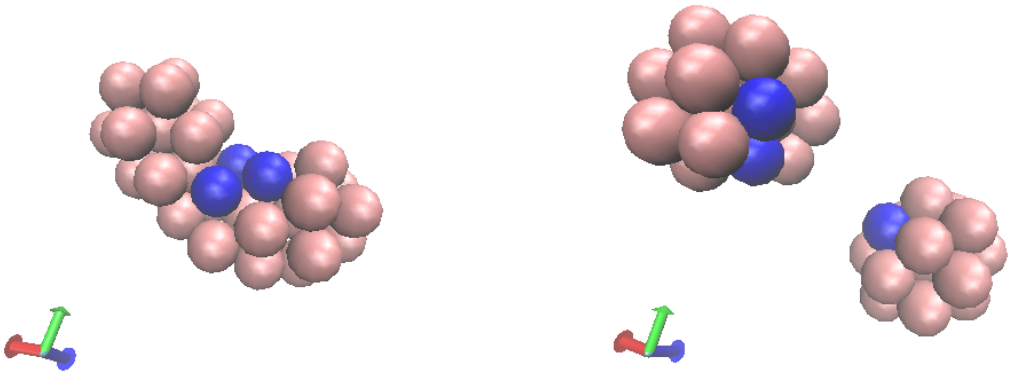

Figure 16: Banana shaped Ni_3Au_{35} cluster at T=150 K equilibrium step (left) and Ni_3Au_{35}, just after decay, two Ni atoms in one fragment and one Ni atom in the second fragment (right).

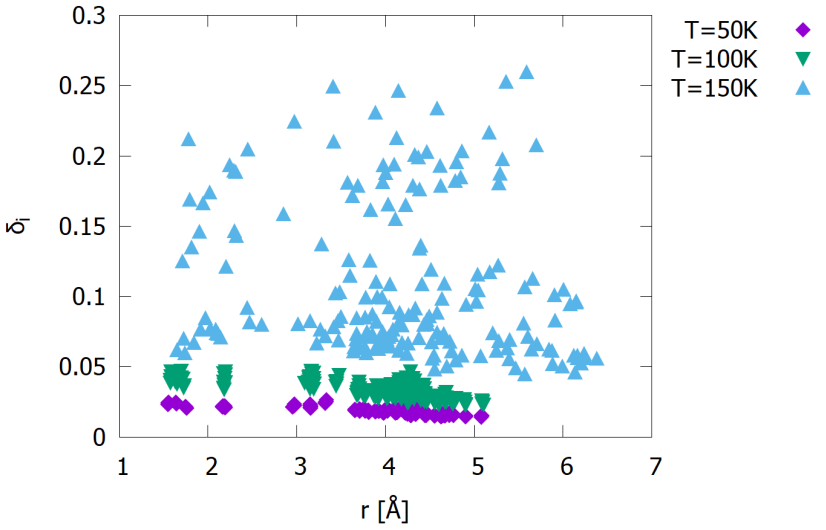

Figure 17: Lindemann index of the Ni_3Au_{35} (130) cluster in a temperature range of 50 K, 100 K and 150 K.

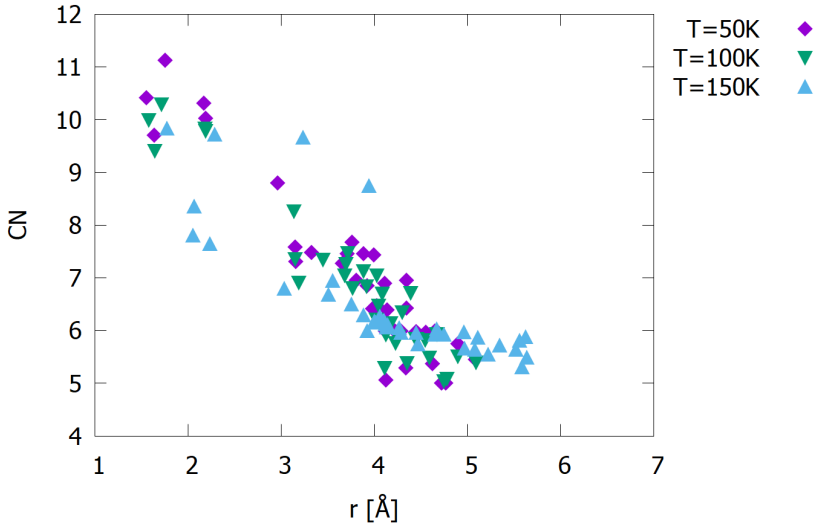

Figure 18: Coordination number CN plotted versus the positions of the atoms the Ni_3Au_{35}-130 cluster, in a temperature range from 50 K to 150 K.

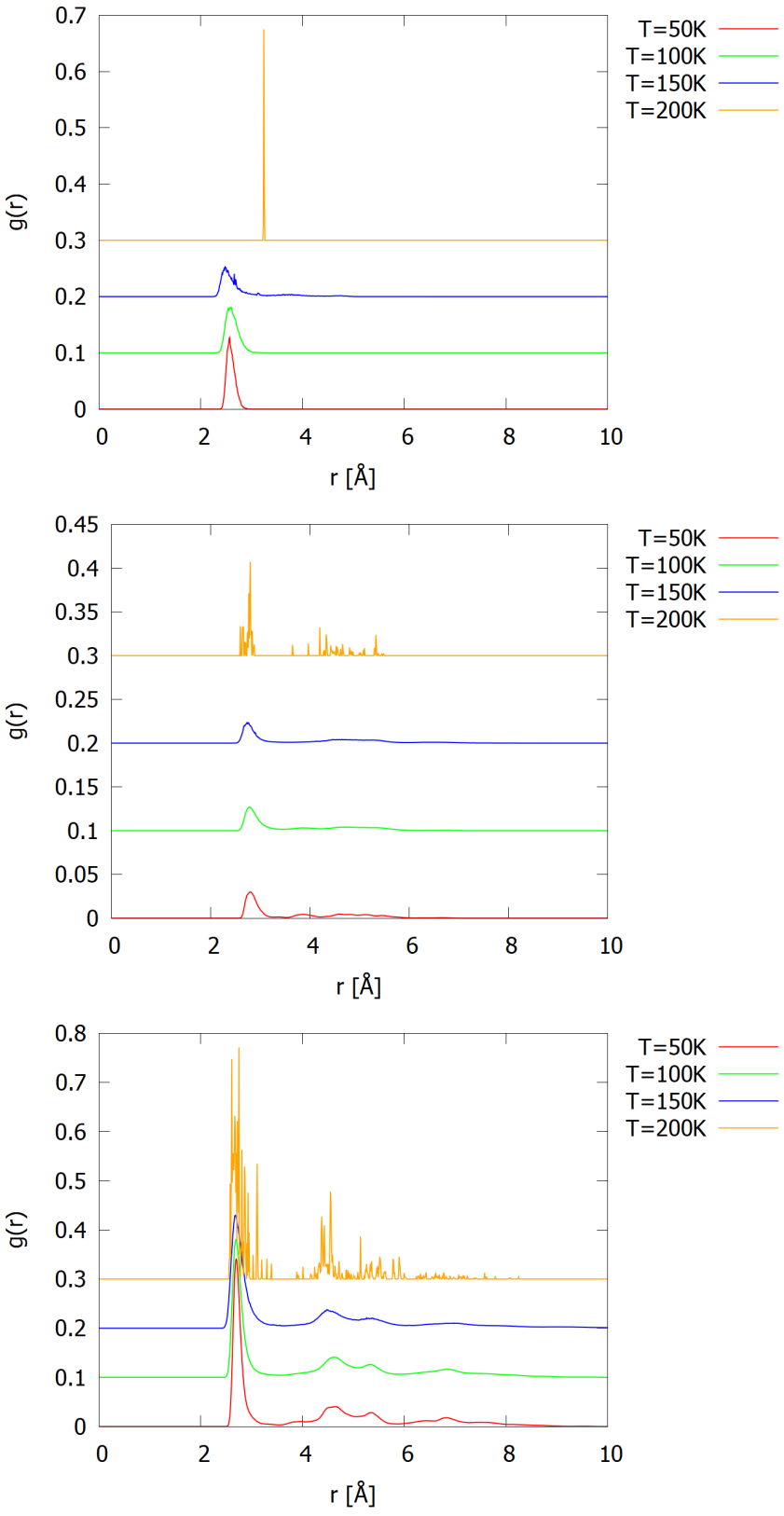

Figure 19: Temperature dependence of the pair distributions of Ni-Ni (top), the Au-Ni (middle) and Au-Au (bottom) for the Ni_3Au_{35}-cluster.

Table 1: Parameters from [16] used in the MD-simulation

Element	A [eV]	ξ [eV]	p	q	r_0 [Å]
Ni	0.0376	1.070	16.999	1.189	$3.523/\sqrt{2}$
Au	0.2061	1.790	10.229	4.036	$4.079/\sqrt{2}$